

# Optical Dipole Nano-Antennas on Glass Substrates

Toni Haugwitz<sup>1</sup>, Jens-Wolfram Erben<sup>2</sup>, Niels Neuman<sup>1</sup>, Danny Reuter<sup>2,3</sup>, Dirk Plettmeier<sup>1</sup>

<sup>1</sup>Chair for RF and Photonics Engineering / Technische Universität Dresden  
01062 Dresden, Germany  
toni.haugwitz@tu-dresden.de

<sup>2</sup>Fraunhofer Institute for Electronic Nano Systems (ENAS)  
09126 Chemnitz, Germany  
jens-wolfram.erben@enas.fraunhofer.de

<sup>3</sup>Center for Microtechnologies / Technische Universität Chemnitz  
09126 Chemnitz, Germany

**Abstract** - In this paper, the results of the successful fabrication as well as the optical backscattering characterization of single plasmonic gold dipole nano-antennas on a six inch quartz glass substrate are shown. For the fabrication of the nano-antenna structures an e-beam lithography lift-off fabrication process has been used. In order to achieve a high structural resolution a bilayer PMMA resist system with different exposure sensitivities and an overall thickness of approximately 300 nm was realized. The manufactured structures were investigated by SEM and AFM imaging and characterized by optical confocal backscattering measurements. The realized samples meet the target nano-antenna geometry (bar shape) in principle, but there is a significant increase in the dipole width of almost 50 nm up to 100 nm compared to the 50 nm target width whereas the target aspect ratio of five is strongly reduced. Additionally, the target metallization thickness of 25 nm is reduced by up to 10 nm which leads to a redshift of the optical scattering resonance of almost 150 nm. A confocal measurement setup designed in the frame of this work together with electromagnetic modeling allows the investigation of these deviations effects. The measured wavelength dependent scattering response matches well the theoretical FEM based simulation results taking into account the actual geometry.

**Keywords:** optical nano-antenna, e-beam lithography, plasmonics, far-field-to-near-field transducer, nanophotonics

## 1. Introduction

Optical nano-antennas based on plasmonic effects represent a class of optical structures that allow bridging the interfacing mismatch between micro- and nanophotonics [1]. Their ability to strongly confine far-field radiation in the vicinity of dielectric-metallic interfaces and the associated near-field enhancement far below the diffraction limit enable optical far- to near-field transducers and vice versa [2]. This allows an efficient interaction between optical nanoelements (such as quantum dots, fluorophores, etc.) and far-field radiation. By using different nano-antenna geometries [3,4] and structural modifications, various nano-antenna properties (e.g. emitted optical polarization state, near-field coupling efficiency, emission rate [5-8], directivity [9,10]) can be altered. However, the precise fabrication of nano-antennas with dimension below 500 nm as well as the integration in semi-conductor technologies is still a challenge.

In this publication, the focus is on the fabrication and characterization of a simple gold based dipole nano-antenna on a six-inch quartz glass wafer with an e-beam lithography lift-off fabrication scheme. This process is intended to be compatible with standard semiconductor fabrication. Usually, ITO (indium tin oxide) coated glass substrates are used to reduce e-beam charging phenomena on the surface [11]. In contrast, we used an additional metallization of the photoresist to achieve this effect. The complete scheme of the e-beam lift-off fabrication and the optical characterization method are introduced in Section 2. In chapter 3, some characterization results of SEM and AFM imaging are shown and discussed. Subsequently, FEM based electromagnetic simulation results of the spectral scattering response are given and compared with the measurements. In the last section, the results are summarized.

## 2. Materials and Methods

The optical nano-antenna structures were fabricated on a six inch quartz glass wafer (semiconductor grade) with a thickness of 675  $\mu\text{m}$  (SEMI standard) by means of an e-beam lithography lift-off process. As shown in Figure 1 (left), the surface quality of the used glass wafers is insufficient. Although the RMS value of the roughness is below 1 nm for the whole wafer (as stated by the manufacturer) local areas show large deviations which can impair the nano-antenna fabrication. Anyway, in the first step the cleaned and dehydrated glass wafer was coated with a quasi-monolayer HMDS (Hexamethyldisilazane) film to provide a defined adhesion for the following photoresist layer. This is a common wafer surface treatment which is used to convert the hydrophilic glass substrate surface to a hydrophobic surface to prevent a delamination of the photoresist during the subsequent wet etching. Following this, a bi-layered PMMA (Poly(methyl methacrylate)) photoresist film with individual exposure sensitivities (layer with lower sensitivity on top) were spin coated onto the wafer with a complete thickness of approximately 295 nm, see Figure 1 (center, (a)). This photoresist configuration provides an undercut resist profile and ensures that no sidewall metallization should occur. To reduce surface charging effects which potentially decrease the achievable structural resolution due to the poor conductivity of the glass substrate during the e-beam writing step, the photoresist was subsequently sputtered with a 20 nm thick gold metallization (b). Furthermore, this metallization provides a highly reflective surface which is helpful for the optically controlled wafer height alignment procedure. After the e-beam exposure step (c) of the photoresist, the metallization was removed by wet etching with a subsequent development of the photoresist (d). In the next step, a metallization consisting of 3 nm chromium as an adhesion layer and 25 nm gold was sputtered again onto the wafer (e). The remaining resist has been stripped by means of an ultrasonic assisted acetone bath to uncover the structures (f).

The measurement setup for the spectral backscattering characterization of single optical nano-antennas consists of a confocal optical microscope configuration (see Figure 1 (right)) [12,13]. A super continuum (SC) white light laser source (Leukos SM-30x) in combination with a reflective optical blazed grating (1200 lines per millimeter) on a piezo driven rotation stage for the white light wavelength splitting has been used. In order to improve the focusing capability of the beam and providing a well-defined Gaussian beam profile on the device under test (DUT), the optical beam was coupled into a single mode optical fiber (Nufern 780-Hp) with an off-axis mirror based collimator (C1) which is used as aperture for the wavelength separation and as spatial filter. The calibration of the spectrum was carried out with an optical spectrum analyzer (Yokogawa) and the spectral resolution was found to be less than 5 nm. After the beam collimation with a second off-axis mirror (C2) and passing a polarization as well as power control unit consisting of broadband linear polarizers and a broadband half-wave plate, the beam was chopped for the homodyne detection. We used an objective lens with a 100 $\times$  magnification and a numerical aperture of 0.9 (Olympus) for the beam focusing onto the DUT. The DUT is mounted on a nanopositioning stage. The backscattered light is collected by the objective lens and passes through a beam splitter (BS) to a detector. The detector is connected to a lock-in amplifier. The LED is used for the illumination of the DUT. The chopper is used for the modulation of the LED light. The LED light is reflected by mirror M3 and passes through a chopper, a half-wave plate ( $\lambda/2$ ), and two polarizers (Pol.) before being reflected by mirror M2. The SC source is reflected by mirror M1 and passes through an optical grating, a collimator (C1), a lens, and a second collimator (C2) before being reflected by mirror M2. The light from the SC source and the LED is combined at mirror M2 and passes through a beam splitter (BS) to the objective lens. The backscattered light is collected by the objective lens and passes through a beam splitter (BS) to a detector. The detector is connected to a lock-in amplifier.

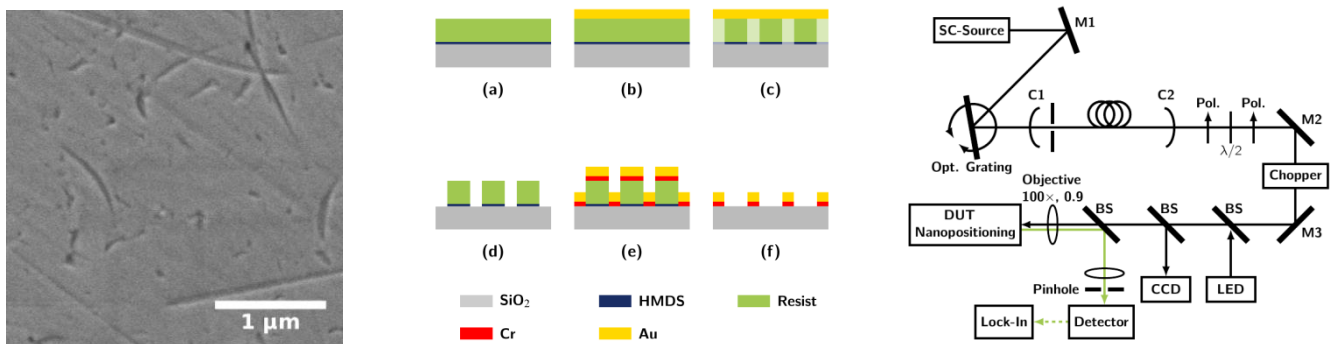


Fig. 1: (left) SEM image of a Carbon-coated wafer sample which clearly shows an insufficient surface quality; (center) Schematic of the used lift-off fabrication process with (a) photoresist spin-coated wafer, (b) deposition of the anti-charging Cr/Au metallization, (c-d) e-beam exposure of the resist followed by Au wet etching and photoresist development, (e) second Cr/Au metallization of the photoresist mask, (f) ultrasonic assisted photoresist stripping to uncover the nanostructures; (right) Optical confocal measurement setup for the spectral backscattering characterization of single optical nano-antennas.

In order to achieve the minimal Gaussian shaped spot size on the DUT, the sample position had to be axially adjusted due to the chromatic dispersion of the objective focal length during the wavelength sweep [13]. The backscattered light from the DUT was separated from the incoming beam by a beam splitter (BS) and focused on a pinhole to suppress ambient light. For detection, a VIS enhanced NIR low noise InGaAs photodetector has been used.

### 3. Results

The manufactured nano-antenna structures show a well-defined racetrack-shaped geometry with a high symmetry between the end caps and quite low side edge roughness (see Figure 2 (a)). The SEM image also shows that the target geometry of the nano-dipoles with a length of 250 nm and a width of 50 nm could not be achieved. The critical dimension (width of the short axis) is increased by a factor up to three. Therefore, the envisaged aspect ratio of five is significantly reduced. AFM imaging was used to determine the height profile of the nanostructures and for a more detailed analysis of the realized geometry (see Figure 2 (b)-(c)). It can be seen that the extracted height map revealed a huge thickness variation and clustering of the gold metallization. Calculating the height distribution as well as the median over the nano-antenna cross-section, the effective metallization thickness is found significantly lower than the target 25 nm.

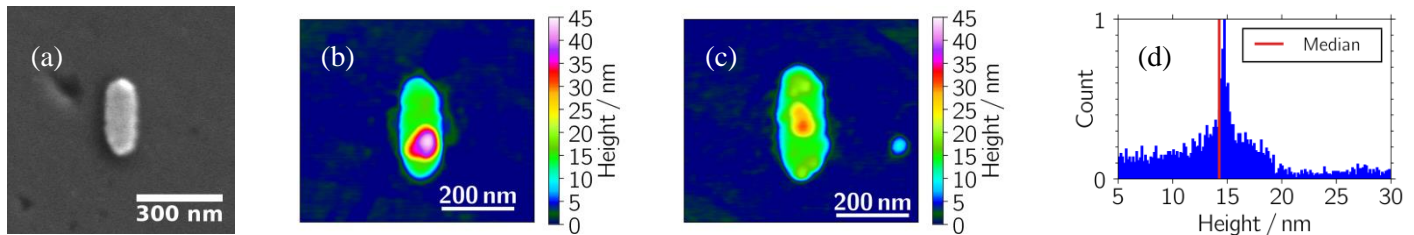


Fig. 2: (a) SEM image of a manufactured nano-antenna; (b-c) AFM height maps of two different nano-antennas showing the issue of the inhomogeneous metallization height distribution and clustering; (d) Histogram of the height distribution of the nano-antenna in (c).

Nevertheless, for the presented sample in Figure 2 (c) the measured spectral behavior (ratio of the backscattered power of the DUT normalized to the pure substrate reflected power) shows the typical Lorentzian-shape of the spectral backscattering with resonance maxima for the long axis close to 1375 nm and for the short axis close to 750 nm (see Figure 3 (a)). The signal fluctuations in the spectral range of 600 nm up to 700 nm are related to the low sensitivity of the used photodetector in this domain (low SNR). Furthermore, the used SM-fiber leads to a mode jump (single- to multi-mode transition) below 780 nm and thus the field profile on the focal plane is no longer a Gaussian distribution. This leads to inhomogeneous illumination of the DUT. We also expect a strongly damped second long-axis resonance in this spectral domain. The small peak close to 1400 nm is due to additional noise caused by the OH-ion absorption within the used optical fiber. Compared to the numerical analysis of the scattering cross-section of the target nano-antenna geometry (see Figure 3 (b)), the measured long axis resonance is redshifted by almost 200 nm. If the geometrical cross-section of the model is adapted to the lateral nano-antenna dimensions extracted from the AFM image, only a slight spectral redshift of the resonance in combination with a decreasing of the resonance Q-factor is observed. Extending and widening the dipole geometry at the same time leads to counteracting effects that minimize the resulting spectral shift of the resonance. The extension of the dipole length causes a redshifts of the resonance wavelength whereas a widening of the dipole width causes a blue shift. Thus, both structural changes provide an opposite effect on the resonance wavelength. A match between measurement and simulation could only be observed when an additional decrease of the dipole height as indicated by the AFM measurements is included in the simulation. In our case, an effective height of 15 nm led to the agreement of measurement and numerical analysis (value was taken from the histogram of the corresponding structure (see Figure 2 (d))).

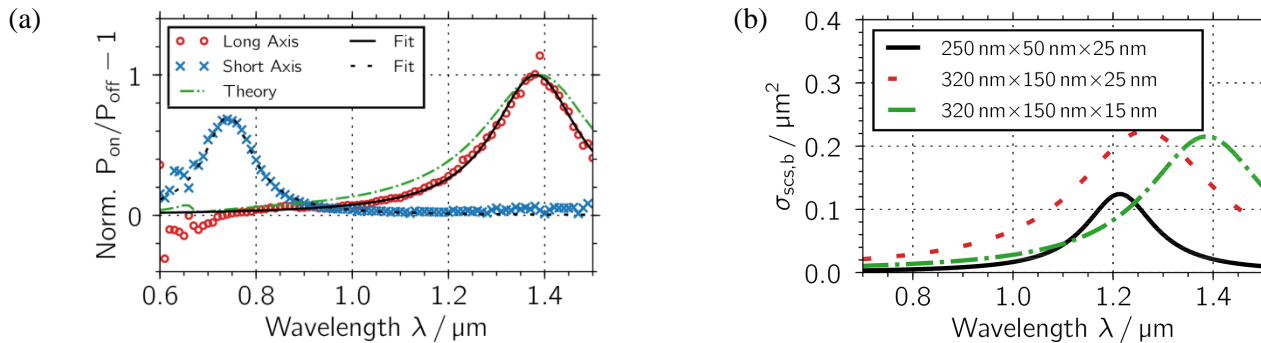


Fig. 3: (a) Measurement (raw data and Lorentzian-fit) and simulation of the backscattering behaviour show two resonance maxima for long and short dipole axis; (b) FEM simulation results of the long-axis backscattering cross-section (backscattered power in the upper hemisphere) for different nano-antenna geometries.

#### 4. Conclusion

Nano-antennas have been fabricated successfully in a process that is compatible with standard semiconductor manufacturing. However, the realized aspect ratio was lower than targeted. The evaluation of the AFM results shows that in addition to the observed deviation from the target geometry, there is also a high variation of the realized nano-antenna geometry over the whole wafer. Two adjacent samples have been presented that were structured with the same e-beam exposure dose. Therefore, we assume that the dose is not the reason for the deviation. Also, a variation of the resist height can be excluded because the structures are placed close together (10  $\mu\text{m}$ ). The resist sensitivity could provide some variations over the wafer. The reduced height of the metallization compared to the target thickness is possibly the result of resist shading effects and the slow closing of the resist opening during the gold deposition which disturbs the gold deposition within the resist-free areas. Because of the low metallization thickness we also observe layer formation effects like nucleation. However, the optical characterization provides excellent measurement results of the spectral dependency of the dipole scattering resonances of both dipole axes. We were able to show that the measured result matches the theoretical prediction very well. With the help of numerical analyzes, it could be shown that the thickness of the metallization has a significant influence on the spectral position of the resonance. This underlines how important a sophisticated measurement setup (as developed within the frame of this work) and thoughtful modeling are. These investigations will help to optimize the nanostructures in the future.

#### Acknowledgements

The authors gratefully acknowledge financial support by the German Excellence Initiative via the German Research Foundation (DFG) Cluster of Excellence “Center for Advancing Electronics Dresden” (cfaed).

#### References

- [1] L. Novotny and N. V. Hulst, “Antennas for light,” *Nature Photonics*, vol. 5, no. 2, pp. 83-90, 2011.
- [2] J. A. Schuller, E. S. Barnard, W. Cai, Y. C. Jun, J.S. White, M. L. Brongersma, “Plasmonics for extreme light concentration and manipulation,” *Nature Materials*, vol. 9, no. 3, pp. 193-204, 2010.
- [3] O. L. Muskens, V. Giannini, J.A. Sánchez-Gil, J.G. Rivas, “Optical scattering resonances of single and coupled dimer plasmonic nanoantennas,” *Opt. Express*, vol. 15, no. 26, pp. 17736–17746, 2007.
- [4] D. Dregely, R. Taubert, J. Dorfmüller, R. Vogelgesang, K. Kern, H. Giessen, “3d optical yagi–uda nanoantenna array,” *Nature Communications*, vol. 2, no. 267, 2011.
- [5] O. L. Muskens, V. Giannini, J. A. Sanchez-Gil, J. G. Rivas, “Strong enhancement of the radiative decay rate of emitters by single plasmonic nanoantennas,” *Nano Letters*, vol. 7, no. 9, pp. 2871–2875, 2007.
- [6] S. Kühn, U. Håkanson, L. Rogobete, V. Sandoghdar, “Enhancement of single-molecule fluorescence using a gold nanoparticle as an optical nanoantenna,” *Phys. Rev. Lett.*, vol. 97, 2006.

- [7] A. Kinkhabwala, Z. Yu, S. Fan, Y. Avlasevich, K. Müllen, W. E. Moerner, “Large single-molecule fluorescence enhancements produced by a bowtie nanoantenna,” *Nature Photonics*, vol. 3, no. 11, pp. 654-657, 2009.
- [8] E. B. Ureña, M. P. Kreuzer, S. Itzhakov, H. Rigneault, R. Quidant, D. Oron, J. Wenger, “Excitation enhancement of a quantum dot coupled to a plasmonic antenna,” *Advanced Materials*, vol. 24, no. 44, 2012.
- [9] J. Li, A. Salandrino, N. Engheta, “Shaping light beams in the nanometer scale: A yagi-uda nanoantenna in the optical domain,” *Physical Review B*, vol. 76, no. 24, 2007.
- [10] A. G. Curto, G. Volpe, T. H. Taminiau, M. P. Kreuzer, R. Quidant, N. F. van Hulst, “Unidirectional emission of a quantum dot coupled to a nanoantenna,” *Science*, vol. 329, no. 5994, pp. 930–933, 2010.
- [11] M. Abb, P. Albella, J. Aizpurua, O. L. Muskens, “All optical control of a single plasmonic nanoantenna ITO hybrid,” *Nano Letters*, vol. 11, no. 6, pp. 2457–2463, 2011.
- [12] K. Lindfors, T. Kalkbrenner, P. Stoller, V. Sandoghdar, “Detection and spectroscopy of gold nanoparticles using supercontinuum white light confocal microscopy,” *Phys. Rev. Lett.*, vol. 93, no. 3, 2004.
- [13] T. Haugwitz, J. W. Erben, N. Neumann, D. Reuter, D. Plettemeier, “Plasmonic dipole nanoantennas on a SiO<sub>2</sub>/Si substrate and their characterization,” in *Silicon Photonics: From Fundamental Research to Manufacturing*, International Society for Optics and Photonics, Strasbourg, France, 2018, vol. 10686.